ChemComm

Chemical Communications

rsc.li/chemcomm

ROYAL SOCIETY
OF CHEMISTRY
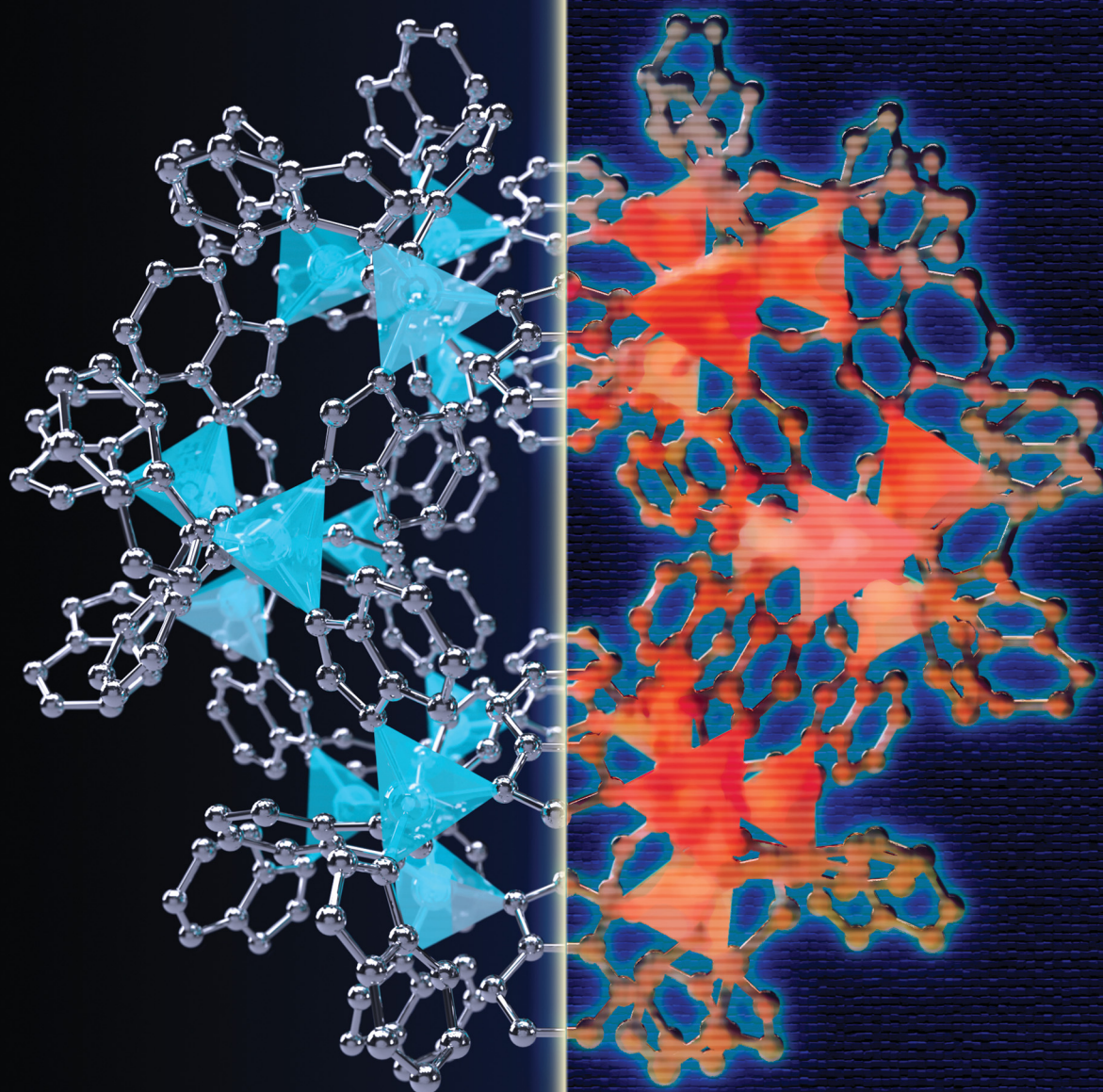
COMMUNICATION
Masataka Ohtani *et al.*
Thermodynamic analysis of gate-opening carbon dioxide
adsorption behavior of metal–organic frameworks

60 YEARS
ANNIVERSARY

ChemComm

COMMUNICATION

Check for updates

Thermodynamic analysis of gate-opening carbon dioxide adsorption behavior of metal–organic frameworks†

Shino Kannaka, Ayumi Ohmiya, Chiho Ozaki and Masataka Ohtani [iD] *

Thermodynamic analysis of gate-opening carbon dioxide (CO_2) adsorption behavior of metal–organic frameworks (MOFs) was investigated using differential scanning calorimetry (DSC). Unlike measurements under nitrogen atmosphere, obvious exothermic and endothermic peaks were observed in DSC curves under CO_2 flow. *In situ* heating X-ray diffraction and thermogravimetric analyses under CO_2 revealed that reversible crystal structure and weight changes occurred upon CO_2 adsorption/desorption. The thermodynamic parameters of the CO_2 adsorption process by MOFs were determined by DSC analysis at various CO_2 partial pressures.

Metal–organic frameworks (MOFs), which consist of alternating coordination bonds of metal ions and organic ligands, can be designed with pore structures. MOFs with pore sizes and shapes that are appropriate for different applications can be produced by changing the combination of metal ions and organic ligands.[1,2] However, the robust structure of most MOFs makes it difficult to control the movement of gas molecules in the pores during gas adsorption and separate mixed gases efficiently. Fortunately, some MOFs are known to change their structure in response to certain stimuli. For example, flexible MOFs with crystalline structures that open up at a certain atmospheric pressure and abruptly adsorb gas molecules have been reported.[3–6] As the pressure decreases, the MOF structures revert to their closed forms, releasing the gas molecules. This gas adsorption behavior, driven by crystal structure changes, is called gate-opening adsorption. The gas adsorption/desorption isotherms of gate-opening MOFs exhibit stepwise adsorption/desorption curves, which cannot be classified by the IUPAC classification for common porous materials.[7] Such behavior can be used for the selective separation of mixed gases because different gas molecules have different threshold pressures for the gate opening of the MOF structure.

School of Engineering Science, Kochi University of Technology, 185 Miyanokuchi, Tosayamada, Kami, Kochi 782-8502, Japan.
E-mail: ohtani.masataka@kochi-tech.ac.jp

† Electronic supplementary information (ESI) available. See DOI: **https://doi.org/10.1039/d3cc05700c**

Zeolitic imidazole framework-7 (ZIF-7) is a well-known MOF that shows structural changes upon adsorption and desorption of carbon dioxide (CO_2).[8–10] ZIF-7 is composed of zinc(II) ions (Zn^{2+}) and benzimidazole (BIm) and has three known crystal polymorphs (phases I, II, and III). These polymorphs have different coordination network structures because of their different bond angles of BIm with Zn^{2+}. Phases I, II, and III of ZIF-7 have rhombohedral, triclinic, and monoclinic crystal systems, respectively. The structure of ZIF-7 changes to phase II upon desorption of *N,N*-dimethylformamide (DMF) from the pores of the phase-I polymorph. Phase I is recovered from phase II by the adsorption of DMF in the closed pores of phase II. These reversible conformational changes of ZIF-7 between phases I and II can also be induced by CO_2 adsorption/desorption.[11,12]

In CO_2 adsorption measurements, ZIF-7 shows a staircase adsorption isotherm as the CO_2 gas pressure changes, which is characteristic of gate-opening MOFs.[13–16] The structural change of ZIF-7 induced by CO_2 adsorption has been examined by *in situ* heating powder X-ray diffraction (XRD).[16,17] The CO_2 adsorption process of ZIF-7 has also been measured under various pressures using synchrotron powder XRD.[18] Kamili *et al.*[19] traced structural changes of ZIF-7 with temperature and pressure using Raman spectroscopy. Molecular dynamics simulations have predicted how CO_2 moves through adsorption sites of ZIF-7.[17,18] In addition, neutron powder diffraction has been used to identify preferential sites of ZIF-7 for CO_2 adsorption.[18,20] Density functional theory (DFT) was used to estimate the thermodynamic energy change required for CO_2 adsorption at each location.[18]

Although the above studies have investigated the relationship between CO_2 adsorption and changes in ZIF-7 crystal structure, this relationship still has many unknown parameters. In particular, the interplay between the CO_2 adsorption process, changes in ZIF-7 structure, and adsorption energy remains unclear. Further detailed experimental investigation of the CO_2 adsorption process by ZIF-7 under atmospheric pressure should be conducted. In this study, differential scanning calorimetry (DSC) is performed under CO_2 atmosphere to evaluate the calorimetric changes accompanying the gate-opening structural
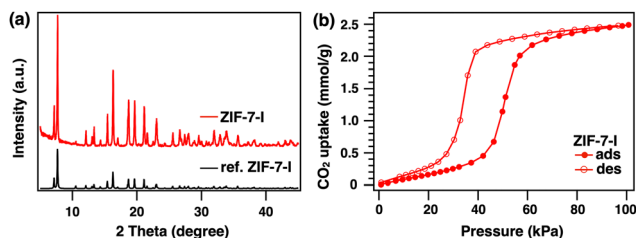
Fig. 1 (a) XRD pattern of as-prepared ZIF-7-I (red) and simulated reference pattern of ZIF-7-I (black, CCDC 602541). (b) CO_2 adsorption/desorption isotherms of ZIF-7-I at 27 °C.

changes of ZIF-7 during CO_2 adsorption/desorption. The behavior of ZIF-7 during CO_2 adsorption/desorption under various conditions is analyzed by DSC to thermodynamically evaluate the adsorption mechanism. Changes in adsorption/desorption behavior associated with structural changes are also followed by *in situ* heating powder XRD and thermogravimetric analysis (TGA) measurements. Furthermore, DSC analysis under various CO_2 partial pressures ($p(CO_2)$) is used to evaluate the thermodynamic parameters of CO_2 adsorption for ZIF-7.

First, the synthetic conditions for ZIF-7 were thoroughly investigated by modifying the literature methods (see the ESI† for details).[12] Fig. 1a shows powder XRD patterns of the ZIF-7 product (denoted hereafter as ZIF-7-I, where I indicates phase I). The observed diffraction peaks were matched to reference peaks, confirming that highly crystalline ZIF-7-I was obtained. Next, CO_2 adsorption measurements were performed to determine the CO_2 adsorption capacity of ZIF-7-I. Prior to the adsorption measurements, DMF in the pores of ZIF-7-I was removed by heating at 200 °C for 20 h. TGA results confirmed the removal of DMF from ZIF-7-I (Fig. S1, ESI†). CO_2 adsorption/desorption measurements were performed at 27 °C. The obtained ZIF-7-I showed CO_2 adsorption/desorption isotherms consistent with gate-opening behavior (Fig. 1b), which rose sharply at a certain pressure. The maximum CO_2 uptake of ZIF-7-I was 2.5 mmol g^{-1}, which was almost identical to that reported in the literature.[14]

To observe the calorimetric change in ZIF-7 caused by CO_2 adsorption, DSC measurements were performed under CO_2 flow (Fig. 2a). Before the measurement, the temperature was increased from 25 to 200 °C at 20 K min^{-1} under a nitrogen (N_2) flow rate of 50 mL min^{-1} to desorb DMF remaining in the pores. The temperature was maintained at 200 °C for 10 min. The temperature was then cooled from 200 to −30 °C at 2 K min^{-1} and subsequently heated from −30 to 200 °C under N_2 flow. No characteristic endothermic or exothermic peaks were observed under N_2 atmosphere (Fig. 2a, blue). After the same pretreatment as for the N_2 measurements, the gas was switched to CO_2 and the same DSC cooling/heating cycle was conducted. Under CO_2 atmosphere, an exothermic peak appeared around 45 °C during the cooling cycle (Fig. 2a, red). In the heating cycle, an endothermic peak was observed around 60 °C. These peaks were ascribed to calorimetric changes originating from the structural changes of ZIF-7-I associated with CO_2 adsorption and desorption. Next, TGA measurements were performed under similar conditions (Fig. 2b). No weight change was
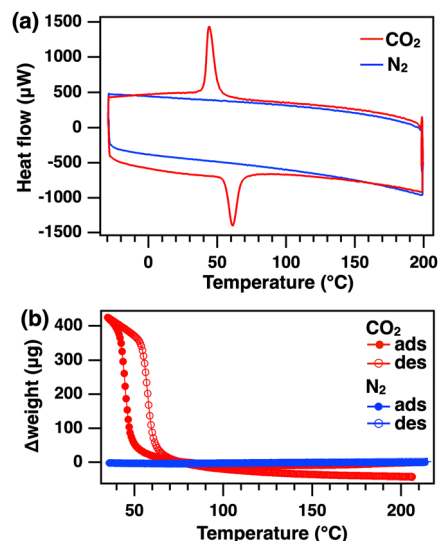

Fig. 2 (a) DSC curves of ZIF-7-I heated at 2 K min^{-1} under CO_2 (red) and N_2 (blue). (b) Thermogravimetric analysis of ZIF-7-I under CO_2 (red) and N_2 (blue).

observed under N_2 atmosphere (Fig. 2b, blue). Under CO_2 atmosphere, weight changes attributed to CO_2 adsorption and desorption were observed during the cooling and heating processes, respectively. These weight changes occurred at temperatures similar to those of the exo- and endothermic peaks in DSC measurements (Fig. 2b, red). These results indicate that the observed calorimetric changes in DSC measurements were caused by the adsorption/desorption of CO_2 on ZIF-7-I.

The calorimetric changes of ZIF-7-I in CO_2 atmosphere were observed repeatedly in DSC measurements (five cycles, Fig. S2, ESI†). The peaks shifted to lower temperature and peak area increased with rising cycle number. Similar behavior was also observed in the TGA of ZIF-7-I in CO_2 (Fig. S3, ESI†). The first cycle showed a large difference between the weight before CO_2 adsorption and that after CO_2 desorption. As the number of cycles increased, this weight difference became smaller. In the first cycle, DMF and other gaseous substances remained in the pores of ZIF-7-I. The slight peak shifts observed in DSC curve and the increasing weight change in TGA curve during cycling are attributed to the gradual desorption of residual solvent and gas molecules. Judging from the negligible weight change upon completion of the fourth and fifth desorption cycles, the repeated weight change, which was accompanied by CO_2 adsorption, was almost complete by the fifth cycle.

The exothermic peak area of the adsorption process was calculated from DSC analysis to be -1.78×10^{-4} kJ. Based on the maximum adsorption amount in CO_2 adsorption/desorption measurements (Fig. 1b) and the isosteric heat of CO_2 adsorption of a typical MOF (25 kJ mol^{-1}), the theoretical adsorption heat was estimated to be -2.69×10^{-4} kJ. Judging from the difference between the observed exothermic heat in the DSC peak area and the predicted exothermic heat, the reaction heat was estimated to be $+0.91 \times 10^{-4}$ kJ. Since ZIF-7 undergoes a significant structural change from close form to open form upon CO_2 adsorption, the
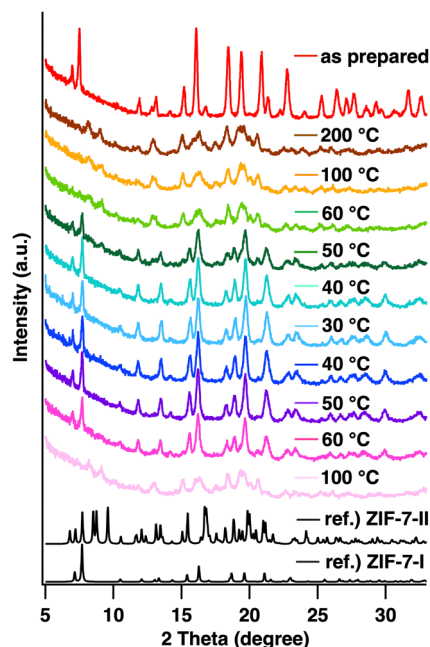
Fig. 3 *In situ* heating powder X-ray diffraction patterns of ZIF-7-I under CO_2 atmosphere. The reference XRD patterns of ZIF-7-I and II were simulated from cif files (CCDC 602541 and 2101613). Patterns were collected during cooling and heating in the following order: as-prepared (red), 200 °C (brown), 100 °C (orange), 60 °C (light green), 50 °C (green), 40 °C (turquoise), 30 °C (light blue), 40 °C (blue), 50 °C (purple), 60 °C (pink), and 100 °C (light pink).

origin of the estimated endothermic heat can be attributed to the reaction heat of the structural change. This indicates that the calorimetric change observed in DSC curve includes both the isosteric heat of CO_2 adsorption and the reaction heat due to the structural change of ZIF-7.

In situ heating powder XRD measurements were performed to confirm the structural changes observed in DSC measurements (Fig. 3 and Fig. S4, ESI†). When heated to 200 °C under N_2 flow, DMF in the pores of ZIF-7-I desorbed and its structure changed to ZIF-7-II. Then, the flow gas was switched to CO_2 and the sample was cooled to 30 °C. The diffraction pattern of ZIF-7-II changed to that of ZIF-7-I at 50 °C, which is consistent with the temperature of the exothermic peak observed in DSC measurements under CO_2. When the sample was heated to 100 °C in the second heating cycle, CO_2 was completely desorbed, and the diffraction pattern indicated that ZIF-7-I converted to ZIF-7-II again. The same measurements were performed under N_2 atmosphere (Fig. S4, ESI†). After the same pretreatment and cooling/heating cycle, no obvious change in the diffraction pattern of ZIF-7-II was observed, indicating that no structural changes occur under N_2 atmosphere. Therefore, the *in situ* heating powder XRD patterns revealed that the calorimetric and weight changes observed in DSC and TGA curves were caused by a gate-opening CO_2 adsorption/desorption process occurring in the crystalline ZIF-7 structure.

Because CO_2 adsorption on ZIF-7 is an equilibrium reaction, we attempted to determine the thermodynamic parameters of this process by changing the CO_2 concentration. For this purpose, DSC measurements were performed with different CO_2 : N_2 ratios (Fig. 4a). As a pretreatment, a series of five

cooling/heating cycles was performed under CO_2. From the sixth cycle, the N_2 : CO_2 ratio was changed for each cycle to decrease $p(CO_2)$. The exothermic peak caused by CO_2 adsorption shifted to the lower temperature side as $p(CO_2)$ decreased. Similarly, the endothermic peak caused by CO_2 desorption also shifted to a lower temperature as $p(CO_2)$ decreased. Since CO_2 adsorption on ZIF-7 is less likely to occur at low CO_2 partial pressures, the adsorption equilibrium temperature is expected to change to a lower temperature. This suggests that changes in $p(CO_2)$ directly influence the chemical equilibrium process of gate-opening CO_2 adsorption by ZIF-7.

Recently, Takiishi and Fujishiro[21] reported the thermodynamic analysis of CO_2 adsorption by cubic perovskite-type $BaFe_{1-x}In_xO_{3-\delta}$. They determined the standard reaction enthalpy and standard reaction entropy from TGA measurements at various $p(CO_2)$, and estimated the standard reaction Gibbs energy change ($\Delta_r G^\circ$) using the obtained parameters. Takamizawa *et al.*[22,23] investigated the DSC behavior of one-dimensional coordination polymer crystals under CO_2 at low temperatures (0 to −35 °C). According to these reports, $\Delta_r G^\circ$ of CO_2 adsorption by ZIF-7-I was estimated from the exothermic peak temperature (T_p) in a series of DSC cooling curves at various $p(CO_2)$. Fig. 4b presents a plot of $\ln p(CO_2)$ against $1000/T_p$, which has a good linear correlation. The slope of the regression line of this plot gave $\Delta_r G^\circ$ = −15.1 kJ mol^{-1}. This experimentally determined value was consistent with the theoretical value obtained from DFT calculations in a previous study.[17] Such thermodynamic parameters are clearly associated with the structural changes of ZIF-7 upon CO_2 adsorption/desorption.

The calorimetric changes in DSC at various CO_2 partial pressures (1.0–0.5 bar) are summarized in Table S1 (ESI†). In the case of lower CO_2 partial pressure, the observed calorimetric changes were slightly greater than that observed at 1.0 bar. As discussed above, since the calorimetric changes in the DSC curve are considered to include the exothermic heat of CO_2 adsorption and the endothermic heat of structural change, it is expected that there is a slight difference in the degree of structural change associated with partial CO_2 adsorption on the crystal surface or in the pore at lower CO_2 partial pressures.

We then measured the DSC behavior of another MOF to examine its ability to adsorb CO_2. Here, we focused on ZIF-9, which is a ZIF-7
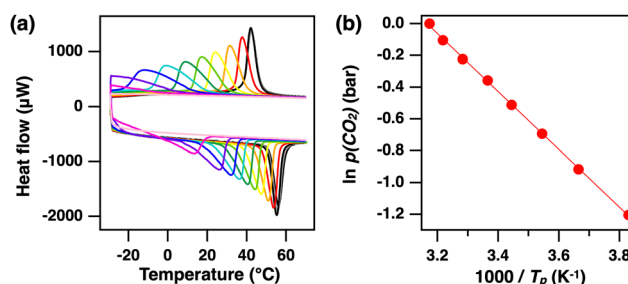

Fig. 4 (a) DSC curves of ZIF-7-I under ambient pressure and different CO_2/N_2 ratios of 1 (black), 0.9 (red), 0.8 (orange), 0.7 (yellow), 0.6 (yellow green), 0.5 (green), 0.4 (light blue), 0.3 (blue), 0.2 (purple), 0.1 (pink), and 0.02 bar (light pink). Above 70 °C is omitted for clarity. (b) Plot of the relationship between the CO_2 partial pressure and exothermic peak temperature (T_p) for ZIF-7-I.
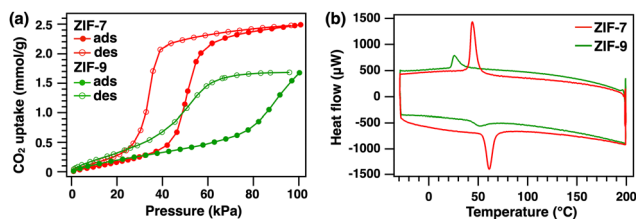
Communication

View Article Online

ChemComm

Open Access Article. Published on 18 March 2024. Downloaded on 12/5/2025 1:57:48 PM.
This article is licensed under a Creative Commons Attribution 3.0 Unported Licence.

Fig. 5 (a) CO_2 adsorption isotherms of ZIF-7 (red) and ZIF-9 (green). (b) DSC curves of ZIF-7 (red) and ZIF-9 (green) heated at 2 K min^{-1} under CO_2.

analog with a similar pore structure (pore diameter (phase II, closed state), ZIF-7: 0.29 nm, ZIF-9: 0.32 nm; pore diameter (phase I, open state), ZIF-7 and ZIF-9: 0.37–0.42 nm)[13–17] that contains cobalt(II) ions rather than Zn^{2+} and also exhibits gate-opening CO_2 adsorption. ZIF-9 was synthesized in a similar manner to ZIF-7 (see the ESI† for details). Powder XRD measurements were performed, and the results were consistent with the formation of ZIF-9 (Fig. S5, ESI†). Fig. 5a shows a CO_2 adsorption/desorption isotherm of ZIF-9 along with one of ZIF-7 for comparison. The total CO_2 uptake for ZIF-9 was slightly lower than that for ZIF-7. The gate-opening CO_2 adsorption process of ZIF-9 was observed at a higher pressure than that of ZIF-7, suggesting that ZIF-9 has a lower CO_2 adsorption ability than that of ZIF-7. DSC measurements were performed for ZIF-9 under the same conditions as for ZIF-7 (Fig. 5b). Exothermic/endothermic peaks ascribed to CO_2 adsorption/desorption were observed for ZIF-9. However, the exothermic peak appeared at a lower temperature than that of ZIF-7, indicating that the CO_2 adsorption ability was lower for ZIF-9 than ZIF-7. Additionally, the DSC peak area for ZIF-9 (-0.71×10^{-4} kJ) was smaller than that for ZIF-7 (-1.78×10^{-4} kJ). This is consistent with the different CO_2 adsorption capacities of the two MOFs identified in their adsorption isotherms. Furthermore, since the estimated exothermic heat of CO_2 adsorption for ZIF-9 based on the adsorption isotherm is -2.00×10^{-4} kJ, the endothermic reaction heat due to the structural change is calculated to be $+1.29 \times 10^{-4}$ kJ, which value is higher than that of ZIF-7. This indicates the intrinsic energy change in the CO_2-induced structural transition of ZIF-9 is greater than that of ZIF-7. These results reveal that DSC under CO_2 is a useful thermodynamic analysis method for exploring the CO_2 adsorption process of MOFs and can be used to quantitatively evaluate various CO_2 adsorption materials.

In conclusion, DSC analysis of ZIF-7 under CO_2 atmosphere was conducted to evaluate its gate-opening CO_2 adsorption behavior. Calorimetric changes associated with the gate-opening structural changes of ZIF-7 occurred only under CO_2. *In situ* heating powder XRD and TGA of ZIF-7 under CO_2 atmosphere revealed that reversible weight and structural changes occurred during CO_2 adsorption/desorption. The thermodynamic parameters of the structural changes of ZIF-7 associated with CO_2 adsorption and desorption were calculated by analyzing the exothermic peak in DSC curves. The evaluation of gas adsorption capacity by DSC presented in this study for ZIF-7 and ZIF-9 is also applicable to other MOFs. The adsorption capacities of different types of MOFs can be compared based on peak areas and temperatures in DSC curves under CO_2 atmosphere. This means DSC is a useful thermodynamic analysis method for evaluating the gas adsorption/desorption

mechanisms of porous materials that undergo related structural changes. We are currently exploring the scope of DSC analysis with other gate-opening MOFs to better understand the thermodynamic parameters of the structural changes in MOFs that exhibit gate-opening gas adsorption behavior.

We acknowledge the financial support from the Japan Society for the Promotion of Science (JSPS) KAKENHI (Grant Numbers 19K05186 and 22K04857). We thank Natasha Lundin, PhD, from Edanz (https://jp.edanz.com/ac) for editing a draft of this manuscript.

Conflicts of interest

There are no conflicts to declare.

Notes and references

1 H. Furukawa, K. E. Cordova, M. O'Keeffe and O. M. Yaghi, *Science*, 2013, **341**, 1230444.
2 S. Kitagawa and R. Matsuda, *Coord. Chem. Rev.*, 2007, **251**, 2490–2509.
3 A. Schneemann, V. Bon, I. Schwedler, I. Senkovska, S. Kaskel and R. A. Fischer, *Chem. Soc. Rev.*, 2014, **43**, 6062–6096.
4 L. Chen, J. P. S. Mowat, D. Fairen-Jimenez, C. A. Morrison, S. P. Thompson, P. A. Wright and T. Duren, *J. Am. Chem. Soc.*, 2013, **135**, 15763–15773.
5 J.-R. Li, R. J. Kuppler and H.-C. Zhou, *Chem. Soc. Rev.*, 2009, **38**, 1477–1504.
6 N. Yanai, K. Kitayama, Y. Hijikata, H. Sato, R. Matsuda, Y. Kubota, M. Takata, M. Mizuno, T. Uemura and S. Kitagawa, *Nat. Mater.*, 2011, **10**, 787–793.
7 S. Hiraide, Y. Sakanaka, Y. Iida, H. Arima, M. T. Miyahara and S. Watanabe, *Proc. Natl. Acad. Sci. U. S. A.*, 2023, **120**, 31.
8 K. S. Park, Z. Ni, A. P. Cote, J. Y. Choi, R. Huang, F. J. Uribe–Romo, H. K. Chae, M. O'Keeffe and O. M. Yaghi, *Proc. Natl. Acad. Sci. U. S. A.*, 2006, **103**, 10186–10191.
9 R. Banerjee, A. Phan, B. Wang, C. Knobler, H. Furukawa, M. O'Keeffe and O. M. Yaghi, *Science*, 2008, **319**, 939–943.
10 M. R. Ryder, B. Civalleri, T. D. Bennett, S. Henke, S. Rudic, G. Cinque, F. Fernandez–Alonso and J.-C. Tan, *Phys. Rev. Lett.*, 2014, **113**, 215502.
11 C. Gucuyener, J. V. D. Bergh, J. Gascon and F. Kapteijn, *J. Am. Chem. Soc.*, 2010, **132**, 17704–17706.
12 P. Zhao, G. I. Lampronti, G. O. Lloyd, M. T. Wharmby, S. Facq, A. K. Cheetham and S. A. T. Redfern, *Chem. Mater.*, 2014, **26**, 1767–1769.
13 X. Wu, M. N. Shahrak, B. Yuan and S. Deng, *Microporous Mesoporous Mater.*, 2014, **190**, 189–196.
14 S. Aguado, G. Bergeret, M. P. Titus, V. Moizan, C. Nieto-Draghi, N. Bats and D. Farrusseng, *New J. Chem.*, 2011, **35**, 546–550.
15 C. M. McGuirk, T. Runcevski, J. Oktawiec, A. Turkiewicz, M. K. Taylor and J. R. Long, *J. Am. Chem. Soc.*, 2018, **140**, 15924–15933.
16 W. Cai, T. Lee, M. Lee, W. Cho, D.-Y. Han, N. Choi, A. C. K. Yip and J. Choi, *J. Am. Chem. Soc.*, 2014, **136**, 7961–7971.
17 Y. Du, B. Wooler, M. Nines, P. Kortunov, C. S. Paur, J. Zengel, S. C. Weston and P. I. Ravikovitch, *J. Am. Chem. Soc.*, 2015, **137**, 13603–13611.
18 P. Zhao, H. Fang, S. Mukhopadhyay, A. Li, S. Rudic, I. J. McPherson, C. C. Tang, D. Fairen-Jimenez, S. C. E. Tsang and S. A. T. Redfern, *Nat. Commun.*, 2019, **10**, 999.
19 K. Kamali, S. Prasad, M. K. Sahoo, J. N. Behera, U. V. Waghmare and C. Narayana, *Inorg. Chem.*, 2022, **61**, 11571–11580.
20 P. Zhao, G. I. Lampronti, G. O. Lloyd, E. Suard and S. A. T. Redfern, *J. Mater. Chem. A*, 2014, **2**, 620–623.
21 K. Takiishi and F. Fujishiro, *J. Phys. Chem. C*, 2022, **126**, 20395–20400.
22 S. Takamizawa, E. Nakata, H. Yokoyama, K. Mochizuki and W. Mori, *Angew. Chem., Int. Ed.*, 2003, **42**, 4331–4334.
23 S. Takamizawa, E. Nakata, T. Akatsuka, R. Miyaki, Y. Kakizaki, H. Takeuchi, G. Maruta and S. Takeda, *J. Am. Chem. Soc.*, 2010, **132**, 3783–3792.

This journal is © The Royal Society of Chemistry 2024

Chem. Commun., 2024, **60**, 4170–4173 | **4173**